MORPHING WING REAL TIME OPTIMIZATION IN WIND TUNNEL TESTS

Andrei V. Popov, Lucian T. Grigorie, Ruxandra Botez

École de Technologie Supérieure, Montréal, Québec, H3C 1K3, Canada

Mahmoud Mamou, Youssef Mébarki

Institute for Aerospace Research, NRC, Ottawa, Ontario, K1A 0R6, Canada

Keywords: Morphing Wing, Real Time Optimization, Wind Tunnel, Laminar-to-turbulence Transition.

Abstract: In this paper, wind tunnel results of a real time optimization of a morphing wing in wind tunnel for delaying the transition towards the trailing edge are presented. A morphing rectangular finite aspect ratio wing, having a wind tunnel experimental airfoil reference cross-section, was considered with its upper surface made of a flexible composite material and instrumented with Kulite pressure sensors, and two smart memory alloys actuators. Several wind tunnel tests runs for various Mach numbers, angles of attack and Reynolds numbers were performed in the 6'×9' wind tunnel at the Institute for Aerospace Research at the National Research Council Canada. Unsteady pressure signals were recorded and used as feed back in real time control while the morphing wing was requested to reproduce various optimized airfoils by changing automatically the two actuators strokes. The paper shows the optimization method implemented into the control software code that allows the morphing wing to adjust its shape to an optimum configuration under the wind tunnel airflow conditions.

1 INTRODUCTION

The Consortium for Research and Innovation in Aerospace in Quebec CRIAQ 7.1 project was a collaborative project between the teams from École de technologie superieure (ETS), École Polytechnique, the Institute for Aerospace Research - National Research Canada (IAR-NRC), Bombardier Aerospace, Thales Avionics. In this project, the laminar flow past aerodynamically morphing wing was improved in order to obtain important drag reductions.

This collaboration called for both aerodynamic modeling as well as conceptual demonstration of the morphing principle on real models placed inside the wind tunnel. Drag reduction on a wing could be achieved by modifications of the airfoil shape which had an effect in the laminar to turbulent flow transition point position. The main objective of this concept was to promote large laminar regions on the wing surface by moving the transition point toward the trailing edge of the airfoil wing, thus reducing drag over an operating range of flow conditions characterized by Mach numbers, airspeeds and angles of attack (Zingg, 2006).

To modify the laminar flow around a wing airfoil, it was necessary to change the airfoil shape; therefore one of the methods for airfoil changes was developed at Kentucky University, which consisted of deflecting the wing upper surface using adaptive actuators (Jacob and Munday, 1998, 1999, 2002).

It was shown that the actuators activated oscillatory motions of a certain frequency to the boundary layer flow over the upper surface. These actuators were made of piezo-electric materials which changed their shapes when connected to an electrical current differential voltage. The wind tunnel tests showed that the displacement of the transition point to the trailing edge resulted in the drag decrease and in the lift increase (Jacob, 1999).

The "chordwise air collection" method was designed in 1984, in fact, laminar flow control (LFC) over the upper surface of the wing was realized by the boundary layer suction, thereby moving the transition position at 85% of the chord (Allison, 1978).

A numerical algorithm was developed for optimizing the suction distribution, by maintaining the transition at a desired location (chord %) and maintaining the energy spent at a minimum (Hackenberg, 1995). Three steps were considered: 1. Boundary layer computation; 2. Transition prediction, and 3. Optimization of the suction distribution while maintaining the transition location at a certain desired percentage of the chord. In the third step, the gradient method was used.

Optimized wings were conceived by reducing the kinetic energy of the perturbation and drag values while, the lift and pitch moment coefficients were maintained at desired values (Pralits, 2003).

A controller was developed at Southampton University, with the aim of maintaining the desired turbulence level over a flat plate equipped with a suction porous panel. The pressure fluctuations were measured with microphones at the boundary layer over the flat plate, and the signal was conditioned and filtered to remove the background noise of the wind tunnel fan, then the turbulence level was estimated by computing the RMS (Root Mean Square) pressure signal. The controller used the error between the RMS values of the measured pressures and the desired RMS values at the spots where the microphones were installed, thus maintaining the transition on the specified area over the flat plate (Rioual, 1994).

Closed-loop control of the morphing planform (wing-shape control) and simultaneously enforced prescribed closed loop aircraft dynamics (flight control) were modeled (Gandhi, 2007). The N-MAS wing designed by NextGen Aeronautics was considered. The flight control law actively used the leading edge morphing wing sweep angle as an actuator to assist in manoeuvres while guaranteeing aircraft stability. The morph between the two modes of Loiter and Dash was modeled by a first-order transfer function, and hence the morph rate was governed by the transfer function time constant.

The empirical structural weights for various wing geometries were obtained by implementing two finite element-based structural optimization methods: 1) an aggregate and 2) a simultaneous analysis (Skillen, 2005). These methods were applied on a morphing wing with two degrees of freedom: the wing sweep and the root chord length. Two linear actuators were used: one positioned along and parallel to the forward spar and the other one positioned along and parallel to the wing root chord. These geometrical variations produced four configurations with changes in area, aspect ratio and sweep: the high lift configuration for the largest area and minimal sweep angle; the loiter configuration for the maximum aspect ratio and minimum sweep angle; the dash/cruise configuration for the maximum sweep and minimal area; and the manoeuvre configuration for the maximum area at the maximum sweep.

A symmetric wing structure was created with two tapered graphite/epoxy composite plates and a steel body. Four pairs of SMA wires were attached to the wings' bottom surfaces in the chord-wise direction. Lift and drag forces were measured at various angles of attack. Dynamic vibration signals were measured by Fiber Bragg Grating FBG sensors at the wing root and were used to monitor aeroelastic unstable flutter phenomena, at various angles of attack (Yang, 2006).

A wing structure comprised of an optimized internal layout of cables and struts was able to change its shape. Cables were used as actuators, while struts provided rigidity to the wing. In addition to achieving continuous morphing by changing cable lengths, this structure had the advantages of being light weighted and having a distributed actuation. Topology optimization was used to optimally place cables and struts in a bay or in a wing section. The Non-dominated Sorting Genetic Algorithm II (NSGA II) was used for modeling the NASA HECS and the NextGen TSCh wings (Bharti, 2006).

Wings roll performances were achieved by use of articulated conformal control surfaces. Analysis results were compared to experimental results obtained for a 16% scale model of a fighter wing equipped with embedded smart materials used to deform a control surface. The control surface design was found suitable for low-rate applications such as takeoff and landing configurations (Sanders, 2003). NextGen developed an in-plane morphing geometry concept. Flexible elastomeric skins with out-of-plane stiffeners accommodated the wing motion while transmitting air pressure loads to the wing substructure. Wind tunnel testing of a full-scale wing for a 2400 lb vehicle and flight testing of a subscale unmanned aerial vehicle (UAV) were performed. The following issues were identified: the need to address multiple geometries and flight envelopes to account for morphing shape changes; the in-plane wing flexibility resulting from its mechanism restraint by linear actuators. Another half-span wind tunnel model was tested in the NASA Transonic Dynamics Tunnel for aeroelasticity studies (Andersen, 2007).

The Flight Test results of a Mission Adaptive Compliant Wing (MAC-Wing) variable geometry Trailing Edge Flap with a Natural Laminar Flow NLF airfoil have been described. The MAC-Wing technology provided light-weight, low power,

variable geometry reshaping of the upper and lower flap surface with no discontinuities. The airfoil-flap system was optimized to maximize the laminar boundary layer extent over a broad lift coefficient range for endurance aircraft applications. The expanded laminar bucket capability allowed the endurance aircraft to extend their range, by 15% or more, by optimizing the lift-to-drag ratio (L/D) throughout the mission. The wing was tested at full-scale dynamic pressure, Mach number, and reduced-scale Reynolds numbers on Scaled Composites' Knight Aircraft. Laminar flow regime occurred up to 60% chord of the wing during tests. Significant fuel and weight savings as well as high control authority were verified by tests and analyses. Fifteen Dantec Dynamics hot film sensors measured the boundary layer transition position (De Breuker, 2007).

A Defense Advances Research Projects Agency DARPA sponsored wind tunnel test model of a Lockheed Martin morphing concept was designed and tested. The wind tunnel model incorporated the key features representatives of a full scale vehicle model: out-of-plane morphing through a coordinated actuation system integrated with seamless skins and a composite support structure that encompassed the actuator system along the wing fold hinge lines, structural layout and materials featured in the full scale vehicle design, and a first-time thermo-polymer actuator integral to a leading edge device for smooth contour between the inner wing and fuselage when fully morphed. The model was instrumented with strain gauges, accelerometers and pressure transducers; data was acquired and correlated with aircraft design and analysis methods (Love, 2007).

The airborne modification of an aircraft wing airfoil shape could be realized continuously to maintain laminar flow over the wing surface as flight conditions changed. To achieve such a full operating concept, a closed loop control system concept was developed to control the flow fluctuations over the wing surface with the deformation mechanisms (actuators) (Popov, 2008).

The wing model had a rectangular plan form of aspect ratio of 2 and was equipped with a flexible upper surface skin on which shape memory alloys actuators were installed (Coutu, 2009 and Georges, 2009). Two shape memory alloys (SMA) actuators created the displacement of the two control points on the flexible skin in order to realize the optimized airfoil shapes (Sainmont, 2009).

As reference airfoil, the laminar Wind Tunnel Experimental Airfoil WTEA was used because it was already optimized for laminar flow in the transonic regime; its aerodynamic performance was investigated at IAR-NRC (Khalid, 1993). The optimized airfoils were previously calculated by modifying the reference airfoil for each airflow condition as combinations of angles of attack and Mach numbers such that the transition point position was found to be the nearest as possible to the airfoil trailing edge (Sainmont, 2009). Several optimized airfoils were found for the airflow cases combinations of Mach numbers and angles of attack. The optimized airfoils configurations were stored in the computer memory by means of a database and were selected as needed by the operator or computer in order to be realized by the morphing wing (Popov, 2009). But this strategy relied on the previously calculated aerodynamic characteristics of the airfoils which usually were determined by use of CFD codes and optimization algorithms.

The idea presented in this paper was to implement the same optimization algorithm into the computer controller that would search the optimal configuration with the real system, in real time and for real aerodynamic airflow conditions. The basic idea of optimization control is to by-pass the necessity of a previously calculated optimized airfoils database, and to generate in real time the optimized airfoil for the exact conditions of the wind flow. For such a task it was necessary to develop a subroutine that optimized the airfoil shape in the same way in which the optimized airfoils database was generated. The method of optimization used in this case was a mixed method between 'the gradient ascent' or 'hill climbing' method and the 'simulated annealing' which is a meta-heuristic search method.

The 'hill climbing' method is a local search optimization algorithm. It considers a random poor solution, which improves slowly by iterations. When solution cannot be further improved, it becomes the final solution and the algorithm ends. In our case, the searching domain is defined by the actuators displacements as variables, while the cost function needed to be maximized is the transition point position x_{tr}. Normally the function is defined analytically and the maximum is searched along the lines with the maximum local derivatives or gradients. Although 'hill climbing' would be very fast and simple to program, the solution found is not guaranteed to be the global maximum of the entire search domain (Hill climbing, from Wikipedia). Other local search algorithms such as 'stochastic hill climbing', 'random walks' and 'simulated annealing' would overcome this problem. The characteristic of these methods is that the algorithm searches random solutions within the search domain

in order to cover all the possible local maxima and to find the global maximum (Simulated annealing, from Wikipedia).

The reason why a mixed method was needed, was because the cost function for such complex problem (minimize the CD, maximize the CL/CD or maximize the transition point position xtr for a morphing wing) was not defined analytically and the implementation of 'gradient ascent' method was not suitable. Also, due to time cost (very long time response of the SMA actuators due to heating but especially cooling time), a purely probabilistic meta-heuristic search algorithm such as 'stochastic hill climbing', 'random walks' and 'simulated annealing', was not suitable too.

The idea of the present algorithm was the mixture of the 'hill climbing' method with the 'random walks' or 'simulated annealing' and the search within the defined domain nine points, one being the center of a circle while the other eight being situated on the circle with a predefined radius. When the maximum is found within the nine points, the algorithm reset the next searching step by iterating with eight points situated on smaller circles until the global maximum is found. This mixed method was found to be the fastest i.e. it considered the least number of points evaluated for converging to the transition point position x_{tr} maximum.

2 EXPERIMENTAL SETUP DESCRIPTION

2.1 Mechanical and Electrical Control System

The concept of this morphing wing consisted in a rectangular wing model (chord c = 0.5 m and span b = 2.1 m) incorporating two parts. One fixed part was built in aluminum by the IAR-NRC team which sustained the resistance forces acting during wind tunnel tests. The other part consisted in a flexible skin installed on a metallic structure on the wing upper surface and was designed and manufactured at Ecole de Technologie Superieure (Fig. 1). The flexible skin was required to change its shape through two action points in order to realize the optimized airfoil for the airflow conditions in which tests were performed.

The actuators were composed of two oblique cams sliding rods span-wise positioned that converted the horizontal movement along the span in vertical motion perpendicular to the chord (Fig. 2).
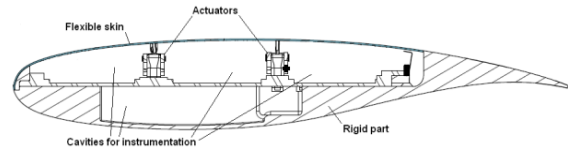

Figure 1: Cross section of the morphing wing model.

The position of each actuator was given by the mechanical equilibrium between the Ni-Ti alloy SMA wires that pulled the sliding rod in one direction and the gas springs that pulled the sliding rod in the reverse direction. The gas springs role was to counteract the pulling effect of aerodynamic forces acting in wind tunnel over the flexible skin when the SMA's were inactive. Each sliding rod was actuated by means of three parallel SMA wires connected to a current controllable power supply which was the equivalent of six wires acting together. The pulling action of the gas spring retracted the flexible skin in the undeformed-reference airfoil position, while the pulling action of the SMA wires deployed the actuators in the load mode i.e. morphed airfoil in the optimized airfoil position (see Fig. 2). The gas springs used for these tests were charged with an initial load of 225 lbf (1000 N) and had a characteristic rigidity of 16.8 lbf / in (2.96 N / mm).
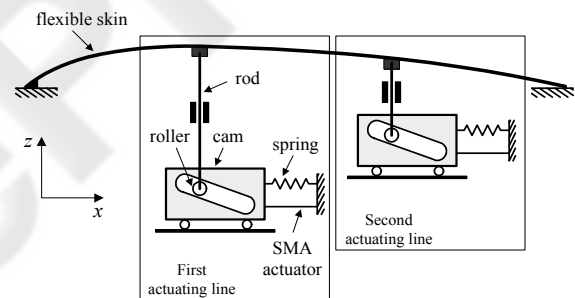

Figure 2: Schematics of the flexible skin mechanical actuation.

The mechanical SMA actuators system was controlled electrically through an "open loop" control system. The architecture of the wing model open loop control system, SMA actuators and controller is shown in Figure 3. The two SMA actuators had six wires each, which were supplied with power by the two AMREL SPS power supplies, controlled through analog signals by the NI-DAQ USB 6229 data acquisition card. The NI-DAQ was connected to a laptop through an USB connection. A control program was implemented in Simulink which provided to the power supplies the needed SMA current values through an analog signal as

shown in Figure 3. The control signal of 2 V corresponded to an SMA supplied current of 33 A. The Simulink control program used as feedback three temperature signals coming from three thermocouples installed on each wire of the SMA actuator, and a position signal from a linear variable differential transducer (LVDT) connected to the oblique cam sliding rod of each actuator. The temperature signals served in the overheat protection system that disconnected the current supply to the SMA in case of wire temperature passed over the set limit of 120°C. The position signals served as feedback for the actuator desired position control. The oblique cam sliding rod had a horizontal versus vertical ratio 3:1; hence the maximum horizontal displacement of the sliding rod by 24 mm was converted into a maximum vertical displacement of the actuator and implicit of the flexible skin by 8 mm.
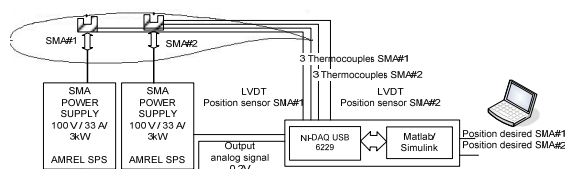

Figure 3: Architecture of the morphing wing model control system.

A user interface was implemented in Matlab/Simulink which allowed the user to choose the optimized airfoils shape from database stored on the computer hard disk and provided to the controller the vertical needed displacements in order to obtain the desired optimized airfoil shape. The controller activated the power supplies with the needed SMA current values through an analog signal as shown in Figure 3. In practice, the SMA wires were heated at an approximate temperature of 90°C with a current of 10 A. When the actuator reached the desired position the current was shut off and the SMA was cycled in endless heating/cooling cycles through the controller switching command on/off of the current in order to maintain the current position until another desired position or the entire system shut off was required.

In support of the discrete pressure instrumentation, infrared thermography (IR) visualization was performed to detect the transition location on the morphing wing upper surface and validate the pressure sensor analysis. The transition detection method using IR was based on the differences in laminar and turbulent convective heat transfer coefficient and was exacerbated by the artificial increase of model-air flow temperature

differences. In the resulting images, the sharp temperature gradient separating high temperature (white intensity in image) and low temperature (dark intensity) regions was an indication of the transition location. The infrared camera used was an Agema SC3000 camera, equipped with a 240×320 pixels Quantum Well Infrared Photodetector (QWIP detector), operating in the infrared wavelength region of 8-9 μm and cooled to 70°K to reduce thermal noise. The camera provided a resolution of 0.02ºC and a maximum frame rate of 60 Hz. It was equipped with the default lens (FOV = 20°×15°), and was installed 1.5 m away from the model with an optical axis oriented in the horizontal plane at about 30° with respect to the wing surface mid-chord normal. Optical access was provided through an opening on the side wall of the test section opposite to the upper surface. More details about the methodology and processing are available in ref. (Mébarki, 2009).

2.2 Aerodynamic Detection System and Graphical User Interface

The morphing wing goal was the improvement of the laminar flow over the upper surface of the wing. In order to ensure that the improvement was real, we built a detection system that gave information about the flow characteristics. An array of twelve Kulite pressure sensors was installed on the flexible skin.

The pressure data acquisition was performed using a NI-DAQ USB 6210 card with 16 analog inputs, at a total sampling rate of 250 kilo samples/s. The input channels were connected directly to the IAR-NRC analog data acquisition system which was connected to the twelve Kulite sensors. The IAR-NRC served as an amplifier and conditioner of the signal at a sampling rate of 15 kilo samples/s. One extra channel was used for the wind tunnel dynamic pressure acquisition to calculate the pressure coefficients Cp's from the pressure values measured by the twelve pressure sensors. The signal was acquisitioned at sampling rate of 10 kilo samples/s in frames of 1024 points for each channel which allowed a boundary layer pressure fluctuations fast Fourier transform (FFT) spectral decomposition up to 5 kHz for all channels, at a rate of 9.77 samples/s using Matlab/Simulink software. The plot results were visualized in real time on the computer screen in dedicated windows (see Figure 4) at a rate of 1 sample/sec. Figure 4 shows an example of graphical user interface in which all the aerodynamic and morphing shape information were centralized together with the control buttons of the controlling

software. The window shows information about the Mach number, the angle of attack, the airfoil shape of the morphing wing, and the two actuators vertical displacements needed to obtain the desired airfoil shape. In the two plots, are shown the pressure coefficients distribution Cp's of the twelve Kulite sensors, and the noise of the signal (RMS) of each pressure signal. Figure 4.a shows the wing un-morphed position, while the Figure 4.b shows the wing under its morphed position. The results obtained are qualitatively very similar to those obtained in previous studies (Nitcshe, 1989 and Mangalam, 2004).

Figure 4.a: Un-morphed configuration.

The transition between laminar and turbulent flow was detected by means of each pressure signal's root mean square (RMS). The lower RMS plot given in Figure 4 shows the normalized quantity of the pressure signal noise from each Kulite sensor (star points curve). In the example shown in Figure 4, the RMS plot in the un-morphed configuration (Figure 4.a) the transition is shown in the fourth sensor due to the fact that it had the maximum RMS value.

In Figure 4.a, on the GUI was shown an un-morphed airfoil by use of a black color. The actuators reference positions correspond to dY1 = 0 mm and dY2 = 0 mm, the Cp distribution calculated by XFoil for the reference airfoil (black curve), and

the Cp theoretical values of the sensors shown as black circles on the Cp distribution curve.
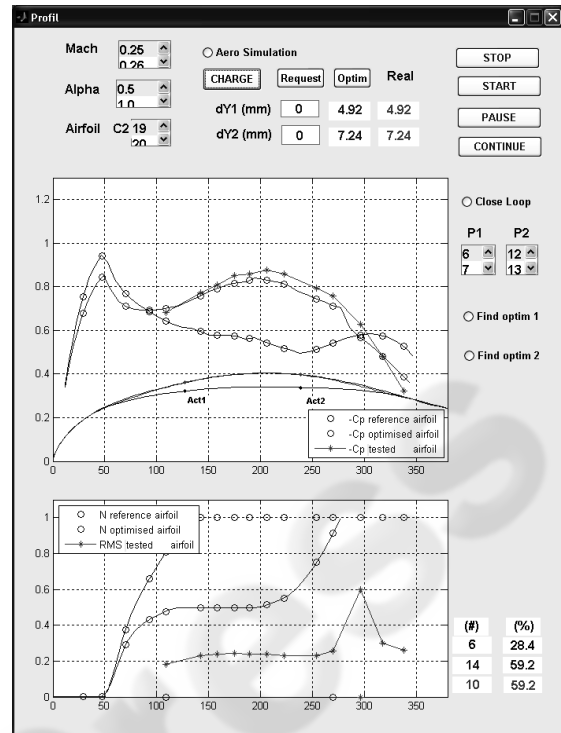

Figure 4.b: Morphed configuration. Graphical User Interface (GUI) with the control buttons of the software.

In the lower plot of Figure 4.a was shown the N factor used by XFoil to predict transition for the reference airfoil (black curve). The critical value N_{cr} = 7.34 was used in the simulation to match the turbulence level T = 0.14% measured in the wind tunnel using Mack's correlation (1), and the plotted values on the figure are normalized (N/N_{cr}) (Mack, 1977).

$$N_{cr} = -8.43 - 2.4 \cdot \log(T) \qquad (1)$$

In the case of an un-morphed configuration, the predicted transition position was found to be the 6th position of the sixteen available sensors positions. In the beginning of wind-tunnel tests, a number of sixteen sensors were installed, but due to their removal and re-installation during the next two wind tunnel tests, four of them were found defective, therefore a number of twelve sensors remained to be used during the last third wind tunnel tests so only twelve Kulite sensors were used for plotting the Cp distribution and RMS distribution (star plots).

Results predicted for the morphed airfoil were shown in circles. The morphed airfoil coordinates were shown as blue curves in the upper part of

Figure 4.b, the Cp distribution was calculated by XFoil for the optimized airfoil (circles curve), and the Cp theoretical values of the sensors were shown as blue circles on the Cp distribution curve. In the lower plot of Figure 4.b, the *N* factor used by XFoil to predict transition was shown for the optimized airfoil (circles curve). In this case of morphed configuration, the predicted position of transition was the 14th position of the sixteen available sensors positions.

These lower circles (un-morphed) and upper circles (morphed) curves served as theoretical validations of the measured value curves reflecting the aerodynamic parameters (Cp and RMS) provided by Kulite sensors in real time with a sampling rate of 1 S/sec. In Figure 4.b is shown the actuated airfoil in the morphed position (dY1 = 4.92 mm and dY2 = 7.24 mm). The transition position was given by the sensor location where the maximum RMS was found, which in this case is the 10th Kulite sensor out of 12 sensors. The instant visualization allows us to find the exact position predicted by XFoil.

2.3 Simulation and Experimental Results Obtained in the Wind Tunnel

The simulation of the system used as programming platform the Matlab/Simulink software. The simulation used the optimization subroutine exactly the same as in bench tests and wind tunnel tests, except that in computer simulation and bench test the aerodynamic pressures that acted upon the skin and which stimulated the sensors were simulated by use of XFoil software. As mathematical model of the flexible skin was used a B-spline with four flexion points. Two points were fixed where the skin is glued on the wing rigid structure and two points were mobile and were placed in the actuators coordinates on the wing structure. The B-spline shape that define the airfoil's flexible skin did not have the same coordinates as the flexible skin but was a good approximation for the purpose of designing an optimization subroutine in closed loop with a CFD code. Laser scanning during bench tests showed that the differences between the scanned airfoils and the theoretical airfoils were less than 0.5 mm (less than 6.25% of the maximum actuators deflection of 8 mm) (Popov, 2009). The optimization initialized the algorithm with the values dY1 = 4 mm and dY2 = 4 mm. Afterwards the algorithm evaluated the transition point position in eight points of coordinates (dY1, dY2) situated on a circle centered in the initial point with a radius of 4

mm within the search domain defined by the bi-dimensional space of actuators strokes {dY1 = [0, 8], dY2 = [0, 8]}. For each evaluation point, the xtr value was evaluated by use of XFoil and stored in the memory. After the first round of evaluations the optimizer decided which evaluating point had the maximum value of xtr, which will became the initial point for the next round of evaluations. The logic schematic of the optimization subroutine is shown in Figure 5.

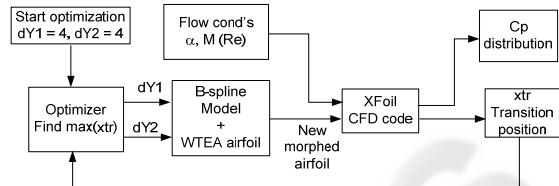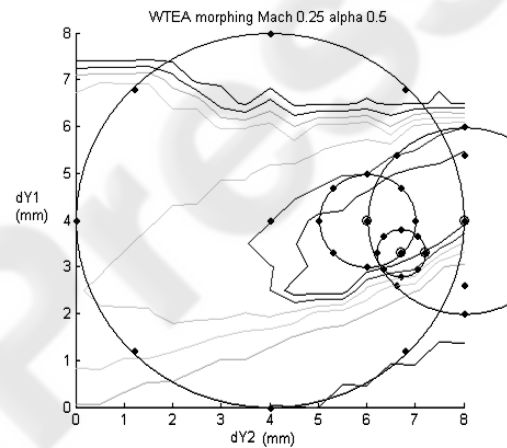Figure 5: Optimization logic schematic.

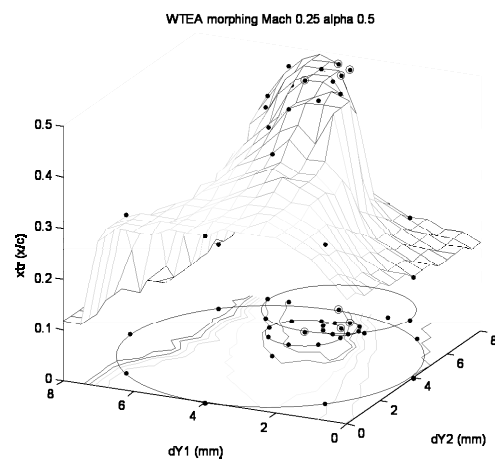Figure 6: Optimization in simulation using XFoil code for the airflow condition $M = 0.25$ and $\alpha = 0.5°$.

Figure 7: Optimization in simulation using XFoil code for the airflow condition $M = 0.25$ and $\alpha = 0.5°$.

Figures 6, 7 and 10 show the result of WTEA airfoil optimization after four evaluation rounds, first evaluation with a radius of 4 mm, second evaluation with a radius of 2 mm, third evaluation with a radius of 1 mm and fourth and last evaluation with a radius of 0.5 mm. As seen in Figure 7 the last round of evaluation was almost unnecessary because the maximum x_{tr} was found inside a plateau of maximums with very small differences between them. Before doing the optimization it was performed a mapping of the search domain, i.e. for each combination of dY1 and dY2 in the interval [0 mm, 8 mm] with a step of 1 mm it was found the xtr and was built the surface $x_{tr} = f$ (dY1, dY2) for the purpose of visualizing the form of the 'hill' and to validate the algorithm in the simulation. Figure 8 and 9 show the same optimization routine that run during the wind tunnel tests in the same airflow conditions as the ones simulated except that there was no map of the searched function. The result was slightly different because the airfoil shape of the real flexible skin under wind tunnel conditions was different than the airfoil shapes defined by use of B-splines. Still the result was similar, in terms of actuator strokes dY1 and dY2 as well as the position of transition. Similarly there could be observed in Figure 9 a plateau of evaluation points that had the transition occurrence on the 11th sensor.

Figure 10 shows the result of the airfoil shape optimization, Cp distribution and xtr transition point position on the upper surface of the airfoil obtained through simulation using XFoil and B-splines model for the flexible skin. The values obtained for wind flow conditions of Mach = 0.25 and a = 0.5 are dY1 = 3.3 mm and dY2 = 7.2 mm. Also in Figure 7 is shown the N factor distribution which was the parameter used by XFoil to calculate the transition point position. When N factor reached the N_{cr} critical value the transition was triggered. This parameter was used in wind tunnel to validate the transition position found through the RMS measuring of the Kulite pressure sensors.

Figure 11 shows the optimized airfoil shape, Cp distribution and xtr transition point position on the upper surface of the airfoil in wind tunnel test (star plots) compared to the optimal airfoil plots (upper circles) and reference airfoil plots (lower circles) obtained through simulation. Also in the lower subplot of Figure 11 the N factor used by XFoil to detect the transition position was compared to the RMS of the Kulite sensors. Both the N factor and RMS were normalized and the purpose of the plots was to have a visual indicator of the transition position. The software considered the transition
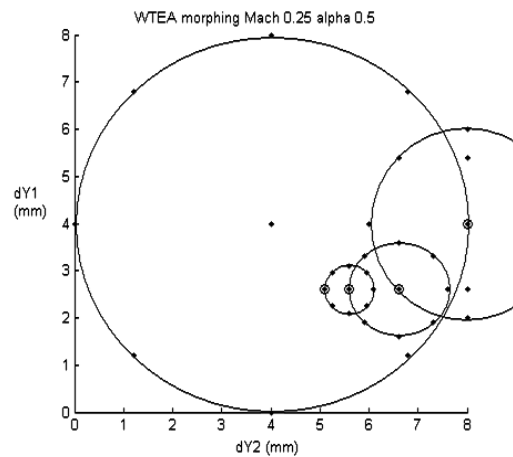

Figure 8: Optimization in real time during wind tunnel tests for the airflow condition $M = 0.25$ and $\alpha = 0.5°$.
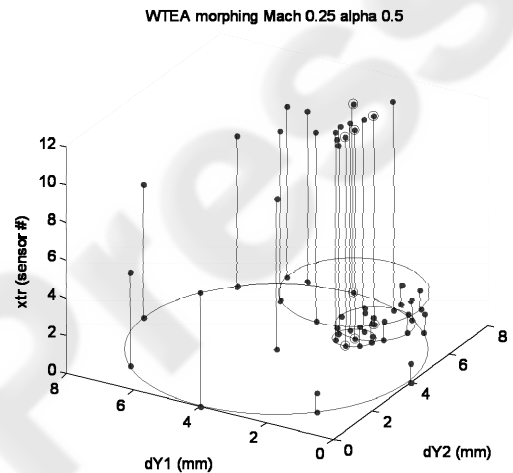

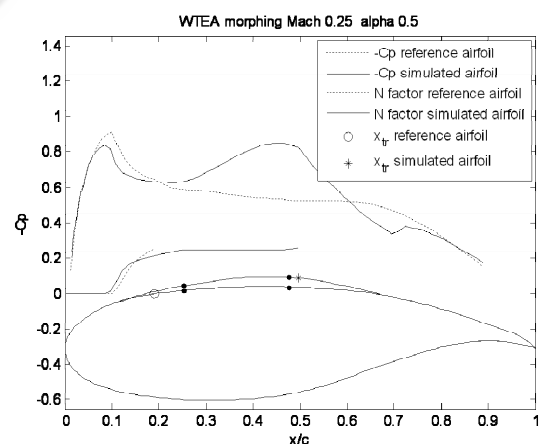Figure 9: Optimization in real time during wind tunnel tests for the airflow conditions $M = 0.25$ and $\alpha = 0.5°$.

Figure 10: Optimization simulation result for M = 0.25 and $\alpha = 0.5°$.

position in the coordinates of the sensor with the highest noise (RMS) as confirmed by previous studies (Rioual, 1994). The values obtained in wind tunnel for wind flow conditions of Mach = 0.25 and a = 0.5 are xtr /c = 0.635 (xtr =317.5 mm) for the actuator displacement values dY1 = 2.6 mm and dY2 = 5.1 mm.
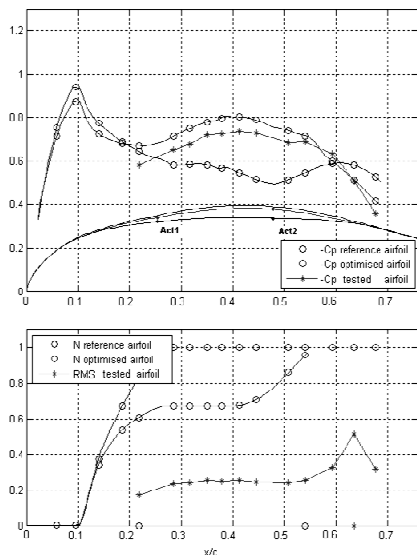

Figure 11: Optimization result during wind tunnel test for M = 0.25 and α = 0.5°.

Figure 12 shows the time history of the optimization process in wind tunnel. Due to the long response of the SMA actuators – the time of cooling from maximum displacement to zero was approx 2 min – the entire process of optimum search converged to the optimum values in approx 20 min. Also, there can be observed that the requested displacements of the actuators at the maximum displacement of 8 mm were not realized, due to the fatigue of the SMA's accumulated in previous testes. The maximum deflection was in fact 7 mm for the first actuator and 6.5 mm for second actuator.

Figure 13 shows typical infrared results obtained at M = 0.25, α = 0.5° for various configurations. Only the composite portion of the wing at x/c≤0.7 was shown. The white spots on the wing are the electronically heated Kulite pressure transducers. The two lines of SMA actuators, colder than the model surface, were also visible at quarter chord and near mid-chord. The locations of the transition in the images have been highlighted using a white dashed line: it corresponded to the location of a large surface temperature gradient, the laminar region being about 2-3°C hotter than the turbulent region.

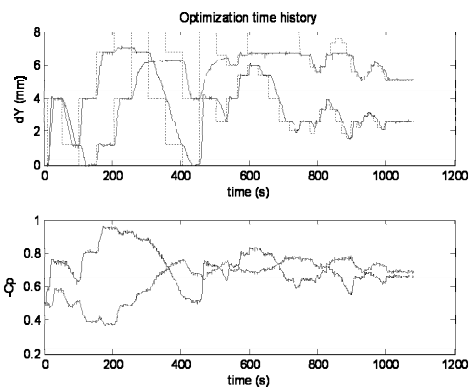The reference airfoil configuration (Figure 13)

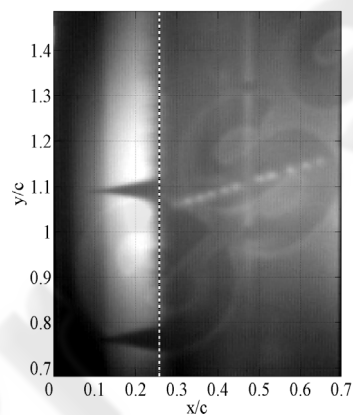Figure 12: Optimization time history during wind tunnel test for M = 0.25 and α = 0.5°.

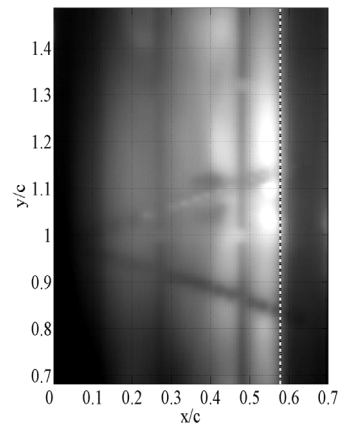Figure 13: Infrared results obtained at M = 0.25 and α = 0.5° in reference position.

Figure 14: Infrared results obtained at M = 0.25 and α = 0.5° after optimization.

showed a transition location at x/c = 26%. The optimization (Figure 14) allowed a laminar boundary layer run to x/c = 58%, which represented a significant improvement over the reference case (Figure 13). Some turbulent wedges caused by

leading edge contamination, due to dust particles in the flow, were visible in Figure 10-a. In addition to providing an on line verification of the Kulite dynamic pressure signals, the infrared measurement was particularly useful to detect those early artificial turbulent regions.

3 CONCLUSIONS

The results of the tests performed in wind tunnel using a morphing wing were shown. The optimization method did not use any CFD code but used the same optimization algorithm in real time. This optimization converged in approximately 10 minutes due to the slow response of the SMA actuators especially in the cooling phase of the cycle. It was observed that the airfoil realized by this method slightly differs from the optimization using CFD codes. This result was due to the fact that the cost function of the optimization (transition position) had discrete values (the sensors positions) and the maximum of the function was a plateau of different dY1 and dY2 values. The optimizer stopped at a certain value in function of the number and magnitudes of the searching steps. It was observed that the last searching step (searching of the maximum in eight points situated on a circle with ray of 0.5 mm – see Figure 9) was not necessary due to the cost function plateau of maximums.

ACKNOWLEDGEMENTS

REFERENCES

Allison, D. O., and Dagenhart, J. R., 1978, Design of a Laminar-Flow-Control Supercritical Airfoil for a Swept Wing, CTOL Transport Technology, NASA Langley Research Center, pp. 395–408.

Andersen, G. R. et al., 2007, Aeroelastic modeling, analysis and testing of a morphing wing structure, AIAA-2007-1734, pp. 359-373.

Bharti, S. et al., 2006, Optimal structural design of a morphing aircraft wing using parallel non-dominated sorting genetic algorithm II (NSGA II), *Smart Structures and Materials 2006: Industrial and Comercial Applications of Smart Structures Technologies*, Proceedings of SPIE Vol. 6166, pp. 1-12.

Coutu, D., Brailovski, V., Terriault, P., 2009, Promising benefits of an active-extrados morphing laminar wing, *AIAA Journal of Aircraft*, Vol. 46(2), pp. 730-731.

De Breuker, R. et al., 2007, Energy-based aeroelastic analysis of a morphing wing, *Proceedings of SPIE*, Vol. 6523, pp. 1-12.

Gandhi, N. et al., 2007, Intelligent control of a morphing aircraft, Paper AIAA-2007-1716, pp. 166-182.

Georges, T., Brailovski, V., Morellon, E., Coutu, D., and Terriault, P., 2009, Design of Shape Memory Alloy Actuators for Morphing Laminar Wing With Flexible Extrados, *Journal of Mechanical Design*, Vol. 131, No. 9, pp. 091006-1–091006-9.

Hackenberg, Petra, 1995, Numerical optimization of the suction distribution for laminar flow control aerofoils, Doctoral Thesis, University of Southampton (United Kingdom).

Hill climbing, From Wikipedia, the free encyclopedia [online], http://en.wikipedia.org/wiki/Hill_climbing

Jacob, J.D., 1998, On the Fluid Dynamics of Adaptive Airfoils, *Proceedings of ASME International Mechanical Engineering Congress and Exposition* November 15-20, 1998, Anaheim, CA, USA.

Jacob, J. D., 1999, Aerodynamic Flow Control Using Shape Adaptive Surfaces, ASME Paper No. DETC99/VIB-8323, *ASME 17th Biennial Conference on Mechanical Vibration and Noise, Symposium on Structronics, Mechatronics, and Smart Materials*, Las Vegas, Nevada, September.

Khalid, M., 1993, Navier Stokes Investigation of Blunt Trailing Edge Airfoils using O-Grids, *AIAA Journal of Aircraft,* Vol.30, No.3, pp.797-800

Khalid, M., and Jones, D. J., 1993 , ACFD Investigation of the Blunt Trailing Edge Airfoils in Transonic Flow, *Proceedings of the Inaugural Conference of the CFD Society of Canada*, Montreal, June14-15.

Love, M. H. et al., 2007, Demonstration of morphing technology through ground and wind tunnel tests, Paper AIAA-2007-1729, pp. 337-348.

Mack, L. M., 1977, Transition and Laminar Instability, *Jet Propulsion Laboratory Publication 77-15*, Pasadena,CA.

Mangalam, S. M., 2004, Real-Time Extraction of Hydrodynamic Flow Characteristics Using Surface Signature, *IEEE Journal of Oceanic Engineering*, Vol. 29, No. 3, pp. 622-630.

Mébarki, Y., Mamou, M. and Genest, M., 2009, *Infrared Measurements of Transition Location on the CRIAQ project Morphing Wing Model,* NRC LTR- AL-2009-0075.

Munday, D., Jacob, J. D., and Huang, G., 2002, Active Flow Control of Separation on a Wing with Oscillatory Camber, AIAA Paper No. 2002-0413, *40th AIAA Aerospace Sciences Meeting*, Reno, NV.

Munday, D., Jacob, J. D., T. Hauser, and Huang, G., 2002, Experimental and Numerical Investigation of Aerodynamic Flow Control Using Oscillating Adaptive Surfaces, AIAA Paper No. 2002-2837, *1st AIAA Flow Control Conference*, St. Louis.

Nitcshe, W., Mirow, P., and Dorfler, T., 1989, Investigations on Flow Instabilities on Airfoils by Means of Piezofoil Arrays, *Laminar-Turbulent Transition Proceedings of the IUTAM Symposium*, Ecole nationale Superieure de l'Aeronautique et de l'Espace, Toulouse, France, Sept. 11-15, , Berlin and New York, Springer-Verlag, 1990.

Popov. A-V., Labib, M., Fays, J., Botez, R.M., 2008, Closed loop control simulations on a morphing laminar airfoil using shape memory alloys actuators, *AIAA Journal of Aircraft*, Vol. 45(5), pp. 1794-1803.

Popov, A-V., Botez, R. M., and Grigorie, L., 2009, Morphing Wing Validation during Bench Tests, *Canadian Aeronautics and Space Institute Annual General Meeting, Aircraft Design & Development Symposium,* 5–7 May, Kanata, Ontario.

Pralits, J., 2003, Optimal Design of Natural and Hybrid Laminar Flow Control on Wings, Doctoral Thesis, Technical Report from Royal Institute of Technology, Stockholm, Sweden.

Rioual, J.-L., Nelson, P. A., and Fisher, M. J., 1994, Experiments on the Automatic Control of Boundary-Layer Transition, Journal of Aircraft. Vol. 31, No. 6, pp. 1416–1418.

Sainmont, C., Paraschivoiu, I., Coutu, D., 2009, Multidisciplinary Approach for the Optimization of a Laminar Airfoil Equipped with a Morphing Upper Surface, *NATO AVT-168 Symposium on "Morphing Vehicles"*, Evora, Portugal.

Sanders, B. et al., 2003, Aerodynamic and aeroelastic characteristics of wings with conformal control surfaces for morphing aircraft, *Journal of Aircraft*, Vol. 40(1), pp. 94-99.

Simulated annealing, From Wikipedia, the free encyclopedia [online], http://en.wikipedia.org/wiki/Simulated_annealing

Skillen, M. D., Crossley, W. A., 2005, Developing response surface based wing weight equations for conceptual morphing aircraft sizing, Paper AIAA-2005-1960, pp. 2007-2019.

Yang, S.-M. , Han, J.-H., Lee, I., 2006, Characteristics of smart composite wing withSMA's and optical fibre sensors, *International Journal of Applied Electromagnetics and Mechanics*, Vol. 23, pp. 177–186.

Zingg, D. W., Diosady, L., Billing, L., 2006. Adaptive Airfoils for Drag Reduction at Transonic Speeds, AIAA paper 2006-3656.

APPENDIX

b = span of wing model (m)

c = chord of wing airfoil (m)

C_D = drag coefficient

C_L = lift coefficient

C_p = pressure coefficient

M = Mach number

N = natural logarithm of rapport between amplified perturbation and initial perturbation in laminar flow

Re = Reynolds number

x_{tr} = transition position (m)

α = angle of attack of the wing (º)